3-22-2010

Bundles of Fluid Fibers Formed by Bent-Core Molecules

C. Bailey
Kent State University - Kent Campus

M. Murphy
Kent State University - Kent Campus

A. Eremin

Wolfgang Weissflog
Kent State University - Kent Campus

Antal Jakli
Kent State University - Kent Campus, ajakli@kent.edu

Bundles of fluid fibers formed by bent-core molecules

C. Bailey,[1] M. Murphy,[1,*] A. Eremin,[2] W. Weissflog,[3] and A. Jákli[1]
[1]*Chemical Physics Interdisciplinary Program and Liquid Crystal Institute, Kent State University, Kent, Ohio 44242, USA*
[2]*Department of Physics, Otto-von-Guericke University, Magdeburg, Germany*
[3]*Institute of Chemical Physics, Martin Luther University, Halle/S, Germany*
(Received 2 January 2010; published 22 March 2010)

The internal structures, stability, and elastic properties of free-standing filament bundles of bent-core smectic liquid crystals are studied using polarizing microscopy, scanning electron microscopy, and a customized cantilever containing, temperature controlled heat stage for force measurements. We find that in bundles, the individual filaments fuse together to form semiseparable filaments with radii approximately two and three times larger than the individual fibers. We also find that the effective surface tension of wide bundles is about 10% smaller than a single filament. Finally, we describe the metastable coexistences of single fibers within the bundles that lead to bending of the bundles. All of these observations were explained with simple macroscopic models.

DOI: 10.1103/PhysRevE.81.031708 PACS number(s): 61.30.Cz, 61.30.Eb, 83.80.Xz, 81.05.Lg

I. INTRODUCTION

Fibers are everywhere in nature and, in many cases, have become commonplace in our everyday life. These fibers are typically formed from a non-Newtonian fluid such as spider webs during their liquid-crystalline phase and optical fibers hardening under a glass transition. For Newtonian fluids and many three-dimensional (3D) liquid-crystalline phases, fluid filaments are only stable when their slenderness ratio (length/diameter) is $S_{3D} \leq \pi$, corresponding to the Plateau-Rayleigh instability [1]. Columnar liquid crystalline phases of disk-shaped molecules [one-dimensional (1D) fluid] can form free-standing fibers even with $S_{1D} \sim 100$ due to their two-dimensional (2D) compressibility [2]. In 2D fluids such as in smectic liquid crystals of rod-shape molecules, $S_{2D}=4.2$, because their 1D layer compressibility was not capable of stabilizing the filament geometry [3]. However recently it was found that some smectic phases of bent-shape molecules ("banana smectics") may also form stable fibers [4,5] with $S_{BS} > 10^3$ [6].

Liquid crystals of bent-core molecules attracted considerable interest when it was observed that they are ferroelectric [7] or antiferroelectric [8], and their structure is chiral without possessing any molecular chirality [8]. The first bent-core materials found to form filaments also formed spectacular helical superstructures such as helical filaments [4,9] under cooling from an isotropic melt. Later it was shown that these materials have modulated smectic structure [10], possibly due to their double tilted polar structure with the molecular plane tilted with respect to the smectic layer normal by an angle θ and with respect the main molecular axis by an angle α. Such a phase was first predicted by de Gennes [11], and was called the SmC_G phase ("G" stands for "general"). For bent-core materials it was reintroduced by Brand *et al.* [12], who predicted that an SmC_G must have an out of layer polarization, which later was verified experimentally [13,14]. In these materials the polarization either cannot be switched, or only at very high (>10 V/μm) fields, possibly via a field induced transition to the single tilted SmCP phase [15], where $\alpha=0$. A theoretical study of the equilibrium size of single free-standing filaments as a function of the angle α found that the stability of the filament increases with larger α [16]. It was also shown that as α approaches $\pi/2$, the layer modulation and filament stability both increase [17]. The most stable bent-core liquid crystal (BCLC) filaments remain stable until the radius decreases below 1.5 μm. In addition, a number of larger BCLC filament bundles can be formed with diameters of 10 μm or larger with slenderness ratios greater than 100 [6]. So far the study of their internal structures and the interaction among the constituent fibers of these bundles were basically neglected. This motivated us to study the physical properties of the bundles of BCLC fibers. With multiple techniques we probe their equilibrium structures, their integration and interactions between the single filaments and explain them with relatively simple macroscopic models.

II. EXPERIMENTS

We studied five different bent-core materials, which we refer to as BC1–5, with molecular structures shown in Fig. 1. BC1–4 [4] have the same nitro-substituted central ring with different alkyloxy terminal chains. In these materials the nitro group presents a steric inclusion leading to a nonswitchable mesophase with modulated layer structures, which (for historical reasons [18]) we label as the B_7 phase. BC5 [19], which has only small steric inclusions due to the small fluorine units, and forms a switchable layer modulated mesophase above an antiferroelectric $SmCP_A$ phase which (for historical reasons [18]) is labeled as B_2. This latter material allows us to compare the filaments in the layer modulated and smooth smectic phases simply by changing the temperature.

Scanning electron microscopy (SEM) images were obtained after pulling filaments in our device, cooling to a crystal phase, then placing the filament on a piece of ITO glass. For better SEM images, the filaments were coated with a thin

*Present Address: Ohio State University, Columbus, OH, USA.

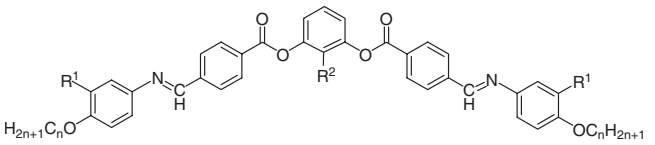

Name	R^1	R^2	n	Phase Behavior (°C)
BC1	H	NO_2	7	Cr 85 B_7 176 Iso
BC2	H	NO_2	8	Cr 116 B_7 177 Iso
BC3	H	NO_2	9	Cr 110 B_7 174 Iso
BC4	H	NO_2	16	Cr 103 B_7 175 Iso
BC5	F	H	10	Cr 110 B_2 147 B_7 160 Iso

FIG. 1. (Top) Basic molecular structure of the bent-core mesogens studied in their filament forms. (Bottom) Name, molecular structures, and phase behavior of studied mesogens.

gold sputtered layer. SEM images were made using a Hitachi S-2600N.

The device that we made to pull and hold the filaments is a self closing tweezers with a tapped hole for use with a screw to open and close the tweezers' tip. The nonopened end of the tweezers is anchored outside of a temperature controlled heat stage (Instec, Inc.) with a mount. This setup and the modified tweezers construction are shown in Fig. 2(a). Images were obtained using a microscope (BX60 from Olympus) and a charge-coupled device (CCD) camera connected to a computer.

The basic experimental setup for the force measurements [see Fig. 2(b)] consists of a heat stage under a microscope where a cantilever is secured and a sealed capillary tube attached to a motorized micropositioner. Force measurements, due to adhesive forces of the fluid filaments connecting the cantilever and capillary tube could be obtained by moving the capillary tube along the x direction and by monitoring the deflection of the cantilever. In the fluid filaments, the surface tension of the liquid-crystal filament adhere the two tips together and by simultaneously monitoring the cantilever deflection and the smallest fluid bridge diameter, the surface tension can be calculated. The cantilever was actually a thin-walled capillary tube of 0.1 mm diameter and about 70 mm length, and is commonly used in x-ray diffraction experiments (Wolfgang Muller GlasTechnik). We obtained the spring constant, $k=0.015\frac{\mathrm{N}}{\mathrm{m}}$, of these cantilevers by measuring the resulting deflection due to applying small masses made of various lengths of string at the cantilever end.

III. EXPERIMENTAL RESULTS

Filament statistics were obtained at constant temperatures by pulling a large number of filaments and measuring their diameters. When a sufficiently large sample number (~100) was collected, statistical properties such as average diameters and size distributions could be created. Comparing the effect of aliphatic tail length and temperature on the average filament diameter for the BC1–4 materials, we see that the diameters decrease with the temperature (see Fig. 3).

We also see that the dependence of the tail length on the diameter of the filament is negligible, suggesting the importance of the molecular core interaction on the formation of filament stability as discussed earlier [17]. This same result was pointed out for the local undulated structure by Pociecha *et al.* [20] by comparing calculated electron density maps and x-ray diffraction pattern for materials with varying tail lengths. Concerning the probability distribution of the fiber diameters at constant temperatures, we also found that the

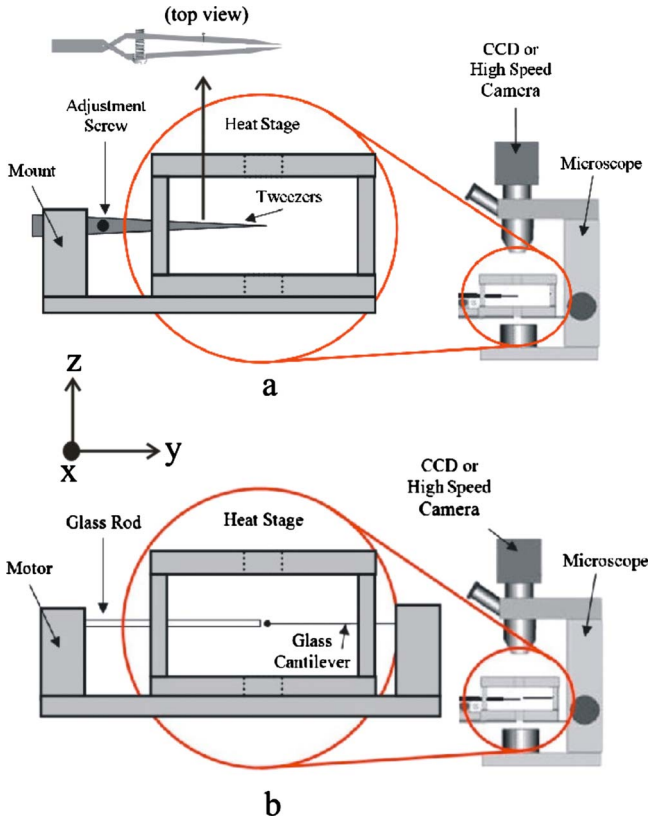

FIG. 2. (Color online) (a) Experimental setup for drawing fibers using a modified temperature controlled heat stage and a polarizing microscope. It consists of a microscope connected to a CCD camera, a customized heat stage with external control of the tweezers' tip spacing. (b) Experimental setup for the cantilever force experiment which consists of a heat stage, a sealed capillary tube attached to a motorized micropositioner and a stationary cantilever.

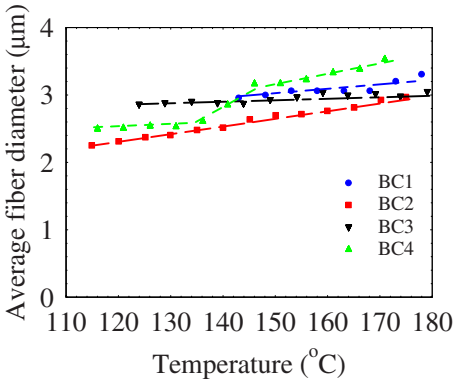

FIG. 3. (Color online) The average filament diameter for the BC1–4 materials as a function of temperature. The behavior shows a weak temperature and no clear aliphatic chain length dependence.

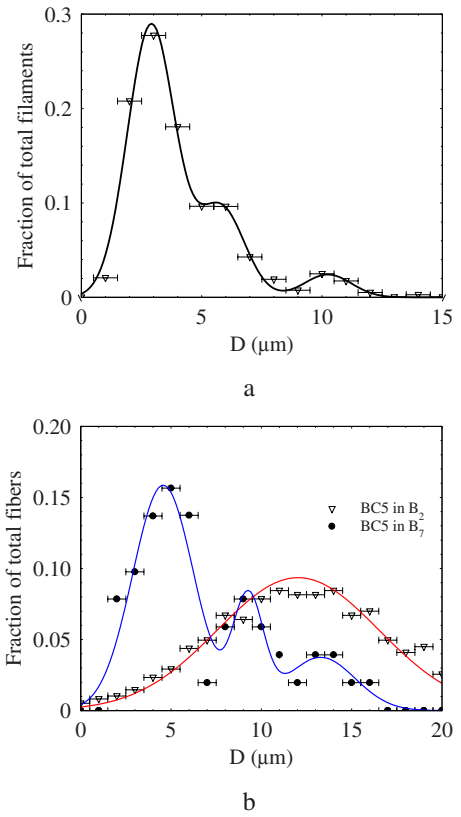

FIG. 4. (Color online) The diameter statistics averaged over 1 μm range. (a) for BC1 in the B_7 range; (b) for BC5 in the B_7, and the B_2 phase along with the best fit curves.

majority of the B_7 filaments have approximately 3–4 μm diameter, but there also exist a relatively large probability of fibers with two and three times larger diameters. Accordingly the distribution function can be fit with a superposition of approximately equally separated Gaussian curves whose peaks decrease with increasing diameter (see Fig. 4). In contrast to this behavior, in the B_2 phase of BC5, we see only a wide peak in the 10–15 μm diameter range [see Fig. 4(b)].

Other interesting observations were made when we pulled multiple filaments in the B_7 phase at a time. In this case sometimes the filaments would bend toward each other and would straighten spontaneously after several minutes. In BC5 this would occur slowly over several minutes, while the same behavior would occur within several seconds in the other materials. The most dramatic effect occurred with the BC3 material when this bending effect was large enough such that the bent filaments touched each other in the middle. PM images of the bending phenomenon for BC5 can be seen in Fig. 5, where we show the coexistence of bent and straight filaments, and the image of the space between the curved filaments between crossed polarizers showing the existence of a birefringent thin film (or a composite of films and filaments) connecting two bundles. This observation shows a metastable coexistence of three different structures consisting of thin films, single filaments, and filament bundles.

To obtain more information about the structures of the thicker filaments, SEM images were taken of the filaments of BC4 drawn near the isotropic—B_7 transition temperature,

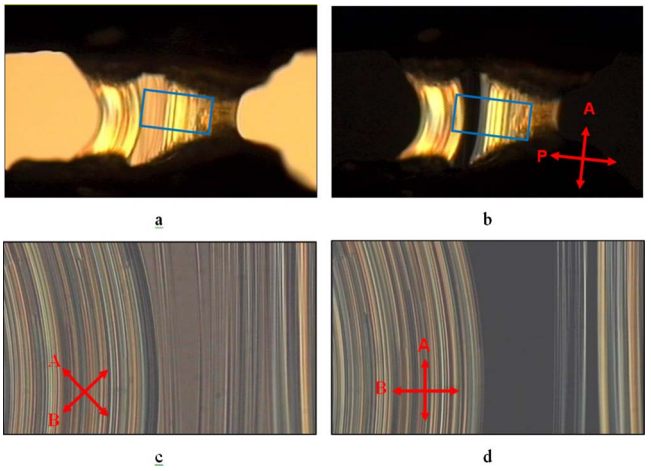

FIG. 5. (Color online) Images of the structures formed during the pulling process for BC5 in the B7 phase. (a) Image of the filament structure without polarizers. (b) Image of the same filament between crossed polarizers aligned along the average filament axis. (c) Image of the region between the bent fiber bundles with crossed polarizers aligned 45° to the average filament axis. We see an extremely thin film or a row of single filaments between two bundles fibers. (d) Image of the region between the bent fiber bundles with crossed polarizers aligned along the average filament axis. We see the thin film (and/or row of single filaments) becomes dark.

then cooled slowly to room temperature through the B_7-crystal transition. Several representative examples are shown in Fig. 6. The first image is of the cross section of an approximately 15 μm diameter filament bundle which appears to have a hole in the center. This hole may be related to a center filament, which broke at a different position than the outer filaments. The second image shows the end of a 5 μm filament with a clean break across its cross section. The third image illustrates the side of a 2 μm diameter filament with an observable helical modulation on the same scale of the filament diameter. This structure resembles the telephone wire structure of B_7 materials observed together with the isotropic melt on cooling [4,21,22]. The last picture shows a bead or pearl defect which has formed by breaking part of a filament bundle which recoils together suspended by the unbroken remaining filament. Normally these beads propagate

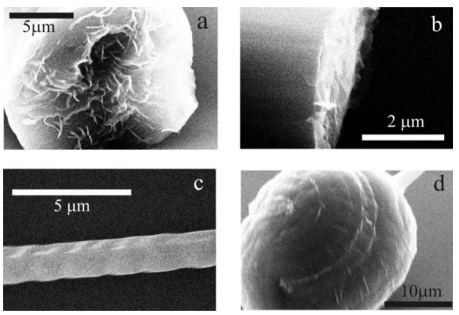

FIG. 6. SEM images of several filaments of BC4 in their crystalline phase. (a) The tip of a broken filament bundle showing a circularly shaped indention; (b) the tip and side of a smaller filament; (c) a thin filament showing helical motif; (d) a bead on the filament showing baseball like pattern on the surface.

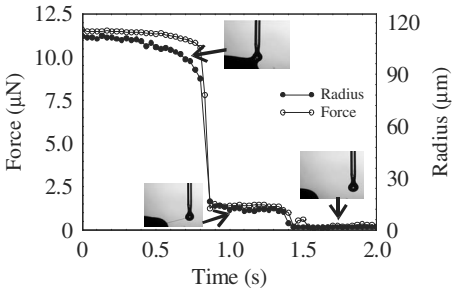

a

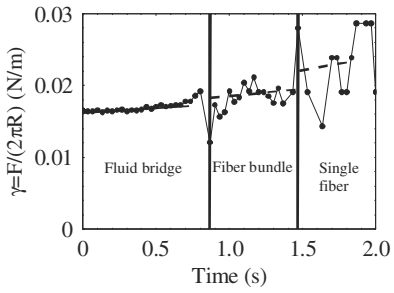

b

FIG. 7. (a) Time dependence of the minimum radius (solid dots, plotted on the right *y* axis) and force (open circles, plotted on the left axis) of a BNC4 filament, as measured in the setup of Fig. 2 by moving the micropositioner by a constant speed. The images illustrate the stages of the pulled material: a bridge of fluid, a bundle of fiber with constant thickness, and a single fiber. (b) The time dependence of the surface tension as calculated from the force and radius curves as $\gamma = F/(2\pi R)$.

to the filament ends, but in this case, the bead was crystallized before this could happen. Even this bulky bead shows a "ball of yarn" pattern suggestive of a tightly coiled filament within the bead.

Force measurements of BC4 near the B_7-isotropic transition were performed using the apparatus shown in Fig. 2(b). By comparing the minimum fluid bridge radius and the measured force determined by the cantilever deflection as shown in Fig. 7, we see that there exists a good correlation between the two sets of data. As the motorized micropositioner moves the sealed capillary tube (the large object at the bottom of the images inset into Fig. 7) with constant speed horizontally to the left, the cantilever is pulled by the bridge and deflects as well. Next, as the fluid bridge begins necking the cantilever relaxes due to the smaller adhesive force. This results in a further necking of the bridge until a stable filament diameter is achieved. This experiment ends when the filament breaks and the cantilever returns to its zero force position.

It can be seen that the reduction in the bridge diameter agrees well with the measured force, except near the transition between the bulk bridge and the fiber structures. This suggests that prior to the fiber formation the bulk fluid moves away from the center of the bridge to the glass surfaces while still holding a constant adhesive force with the glass, probably due to added viscous stresses in the fluid.

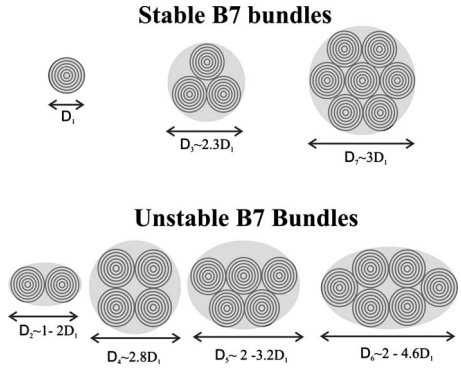

FIG. 8. Model structures of stable and unstable B_7 filaments. The B_7 bundles all contain typically the same 3–4 μm diameter single filaments and bundle to thicker filaments. As experiments show the most stable filaments close-packed with 1, 3, or 7 filaments (see top row) that have the smallest interstitial area, which are bulk materials containing wall defects. The bundles containing 2, 4, 5, and 6 fibers are unstable, because they are asymmetric and the interstitial areas (consequently the surface tensions) are too large.

IV. DISCUSSION

A. Surface tension of the bundles

The measurements with the cantilever techniques on the bundles show that away from the transition point the ratio of the measured force and the bridge circumference $\gamma = \frac{F}{2\pi R}$ provide slightly (but consistently) different surface tensions [Fig. 7(b)]. For very thick ($R_1 \sim 100$ μm) bundles $\gamma_1 \cong 0.018$ N/m; in the thinner ($R_2 \sim 12$ μm) range $\gamma_2 \cong 0.0195$ N/m; and in the single filament ($R_s \sim 2$ μm) fiber, $\gamma_S \approx 0.023$ N/m. Our SEM studies indicate that the individual fibers fuse together, so the interstitial space is not air, but smectic full of defects (grain boundaries) to effectively fill these regions. The energy per length Φ of an interstitial defect can be estimated by recalling that for one grain boundary $\Phi_{GB} \approx \frac{\sqrt{BK}}{\kappa}$ (see Ref. [23]), where $B \sim 2 \times 10^4$ Pa is the effective layer compression modulus, $K = 10$ pN is the Frank elastic constant, and $\kappa^{-1} = 0.5$ μm is an average layer curvature around the defect area, arriving at $\Phi_{GB} \sim 0.2$ nN. For example a hexagonal strand containing seven fibers, the number of defects walls is approximately 12 (see Fig. 8) resulting in $\Phi \sim 2.4$ nN, which is much less that the measured 2 μN of a similar size fiber (see Fig. 7). This shows that the contribution of the defect walls to the free energy is weak, but may explain the slight decrease in the surface tension as the diameter of the bundles and the number of defects increase.

B. Fiber size distribution

The observed fiber size distribution shows that in the B_7 phase, most of the filaments have diameters of roughly 1D, 2D, and 3D (3, 6, and 10 μm for BC1; and 4.4, 9.2, and 13.2 μm for BCN5), with decreasing probability, whereas in the B_2 phase the size distribution is wide with a single peak in the range of 10–15 μm. According to Ref. [16], the size of a single filament is the result of two competing mecha-

nisms: the Plateau-Rayleigh instability modified for non-Newtonian materials [24] with bulk elastic modulus in addition to the surface tension γ that sets a lower limit to the radius; and a steric interaction between molecular cores that induces a spontaneous layer bend that sets an upper limit for the filament radius [16]. The lower limit of the stability can be determined in the same way as derived for columnar liquid crystals [2], resulting in a minimum critical radius $R_c=2\gamma/B$. For typical calamitic smectic liquid crystals, the surface tension is $\gamma\sim 0.02$ J/m^2 and the layer compression modulus, $B>10^5$ J/m^3, so one obtains $R_c<0.4$ μm. For the B_7 materials, filaments rupture below $R\sim 1.5-2$ μm that is about order of magnitude larger than predicted with R_c. As we saw above, and in earlier measurements [6,15], the surface tension of bent-core materials is similar to that of rod-shape materials, which means that the compression modulus should be smaller than usual. Indeed it was shown [16] that in the B_7 phase where the molecular plane can rotate around the director such that $\langle\alpha\rangle>0$, for small layer compressions, the modulus may be biaxial and depend on the polarization as $B_{eff}\approx\frac{P_o^2\sin^2\theta}{\varepsilon\varepsilon_o}+B_c$. In this expression, the first term is due to electric self-interaction of the spontaneous out-of-layer polarization P_o, and $B_c\approx 2-4\times 10^3$ N/m^2 is the difference in the biaxial layer compression modulus. Using reasonable physical parameters, $P_o=200$ nC/cm^2 [25,26], $\theta=\frac{\pi}{6}$, $\varepsilon\varepsilon_0=9\times 10^{-11}$ C^2/J·m^2, we get $B_{eff}=1.6\times 10^4$ N/m^2 and $R_c\sim 2$ μm. Reference [16] also showed that for B_7 materials there is an upper limit of stable filaments R_u, determined by a spontaneous bending tension C, as $R_u=2C/B_{eff}$. It was found [17] that $C\sim 1.5\gamma$, thus giving $R_u\sim 3$ μm, which explains the observed narrow distribution of the single fiber radius to about $2-3$ μm, in agreement with the highest probability radius found experimentally (see Fig. 4). The observed lower probability peaks at twice and three times larger radii therefore correspond to bundles consisting of three and seven fibers, which are more symmetric and allow closer packing (smaller surface area per number of filaments) than bundles with 2, 4 and 5,6,… filaments. These latter fibers require rectangular and other poorly packed structures (see Fig. 8), and they should be asymmetric, so their surface/volume ratio is not minimized.

For the B_2 materials, the situation is different because the molecular plane cannot rotate around the director, but locked at $\alpha=0$. In this case, $B\sim 10^5$ N/m^2 even for small deformations, and the lower limit of stable filament radius $r_c<1$ μm. Indeed in Fig. 4(b) we see that the probability function decreases but does not fall to zero at small radii. At the same time, because $\alpha=0$, there is no upper limit for the filament size explaining why we observed the wide distribution of the filament diameter. On the other hand, we see that the distribution slightly decreases above D~ 10 μm, which indicates that some other mechanism limits the size of the single B_2 fibers, such as viscous effects related to the pulling rate of larger filaments. Another possibility is that the locking to $\alpha=0$ is not completely rigid and that layer bending may introduce a small variation of α. Here we note that large bundles in the B_2 phase were also observed earlier [6] showing much weaker bonding between the B_2 filaments than in B_7.

C. Equilibrium between films/single filaments and bundles

The microscopic observations shown in Fig. 5 about the area between bundles of fibers show multiple important properties. (i) The area is perfectly aligned with optical axis either parallel or perpendicular to the pulling direction; (ii) this area shows thin (~ 2 μm) wide stripes parallel to the drawing direction. Both of these observations indicate that the area is filled by an array of single fibers (ASF). Observation (i) agrees with prior observation on single B7 filaments [6] that found the optical axis to be parallel to the pulling direction. Our observation that ASF makes the surrounding bundles to bend can be qualitatively interpreted as a result of the larger surface tension of the single filament with respect to the bundles (see prior section), which would force the single filaments to decrease their surface area, thus pulling the thicker bundles. Because these situations are not stable, the quantitative interpretation of the shape of the bundles is out of the scope of this paper.

To summarize, we have studied the equilibrium structures of the free-standing filament bundles created from bent-core smectic liquid crystals with polarizing microscopy, by scanning electron microscopy, and cantilever force measurements. We found that in bundles the individual fibers fuse together to composite fibers with radii about twice and three times larger than of the individual filaments. We also found that the effective surface tension of wide bundles is about 10% smaller than of single filaments, which we hypothesize is related to the presence of multiple defects in the bundle. Finally we described metastable coexistences of single fibers with the bundles. All of these observations were explained by simple macroscopic models which suggest that the major factor in the bundle formation is the reduced surface energy compared to that of individual filaments in air.

ACKNOWLEDGMENTS

This work was partially supported by the NSF FRG under Contract No. DMS-0456221 and by NSF IRES Grant No. OISE-0727185. We particularly thank R. Stannarius for his critical notes and helpful discussions. Important technical assistance by Liou Qiu is acknowledged for the SEM measurements.

[1] Lord Rayleigh Proc. London Math. Soc. **10**, 4 (1879).
[2] D. H. Van Winkle and N. A. Clark, Phys. Rev. Lett. **48**, 1407 (1982).
[3] M. P. Mahajan, M. Tsige, P. L. Taylor, and C. Rosenblatt, Liq. Cryst. **26**, 443 (1996).
[4] G. Pelzl, S. Diele, A. Jákli, C. H. Lischka, I. Wirth, and W. Weissflog, Liq. Cryst. **26**, 135 (1999).
[5] D. R. Link, N. Chattham, N. A. Clark, E. Körblova, and D. M. Walba, *Abstract Booklet FLC99* (Darmstadt, University of Darmstadt, Germany, 1999), p.322.

[6] A. Jákli, D. Krüerke, and G. G. Nair, Phys. Rev. E **67**, 051702 (2003).
[7] T. Niori, T. Sekine, J. Watanabe, T. Furukawa, and H. Takezoe, J. Mater. Chem. **6**, 1231 (1996); T. Sekine, T. Niori, M. Sone, J. Watanabe, S. W. Choi, Y. Takanishi, and H. Takezoe, Jpn. J. Appl. Phys. **36**, 6455 (1997).
[8] D. R. Link, G. Natale, R. Shao, J. E. Maclennan, N. A. Clark, E. Körblova, and D. M. Walba, Science **278**, 1924 (1997).
[9] A. Jákli, C. H. Lischka, W. Weissflog, G. Pelzl, and A. Saupe, Liq. Cryst. **27**, 11 (2000).
[10] D. A. Coleman *et al.*, Science **301**, 1204 (2003).
[11] P. G. de Gennes, *The Physics of Liquid Crystals* (Oxford University Press, New York, 1974).
[12] H. R. Brand, P. E. Cladis, and H. Pleiner, Eur. Phys. J. B **6**, 347 (1998).
[13] A. Jákli, D. Krüerke, H. Sawade, and G. Heppke, Phys. Rev. Lett. **86**, 5715 (2001).
[14] A. Eremin, S. Diele, G. Pelzl, H. Nádasi, and W. Weissflog, Phys. Rev. E **67**, 021702 (2003).
[15] R. Stannarius, A. Nemes, and A. Eremin, Phys. Rev. E **72**, 020702(R) (2005).
[16] C. Bailey, E. C. Gartland, and A. Jákli, Phys. Rev. E **75**, 031701 (2007).
[17] C. Bailey and A. Jákli, Phys. Rev. Lett. **99**, 207801 (2007).
[18] G. Pelzl, S. Diele, and W. Weissflog, Adv. Mater. **11**, 707 (1999).
[19] G. Heppke, D. Parghi, and H. Sawade, Ferroelectrics **243**, 269 (2000).
[20] D. Pociecha, N. Vaupotic, E. Gorecka, J. Mieczkowski, and K. Gomola, J. Mater. Chem. **18**, 881 (2008).
[21] G. Pelzl, S. Diele, A. Jakli, and W. Weissflog, Liq. Cryst. **33**, 1513 (2006).
[22] A. Jákli, C. H. Lischka, W. Weissflog, G. Pelzl, and A. Saupe, Liq. Cryst. **27**, 1405 (2000).
[23] M. Kleman and O. D. Lavrentovich, Eur. Phys. J. E **2**, 47 (2000).
[24] J. Prost and N. A. Clark, in *Proceedings of the International Conference on Liquid Crystals*, edited by S. Chandrasekhar (Heyden, Philadelphia, 1980), p. 53.
[25] A. Jákli, G. G. Nair, H. Sawade, and G. Heppke, Liq. Cryst. **30**, 265 (2003).
[26] S. Rauch, P. Bault, H. Sawade, G. Heppke, and A. Jákli, Phys. Rev. E **66**, 021706 (2002).